ORIGINAL ARTICLE

Improvement of thermal plasma sprayed coating adhesion strength by laser microtexturing of aluminum

Anustup Chakraborty[1] · Benjamin Chalfant[2] · John Sions[2] · Ben Zimmerman[2] · Mool C. Gupta[1]

Abstract

Grit blasting and laser processing are two common methods used for surface microtexturing to enhance coating adhesion strength. This paper reports a thermomechanical method of laser microtexturing of Al 7075 alloy using a nanosecond pulsed laser to generate a large increase in surface area. The entire surface area of the substrate was microtextured using laser melting, ablation, and resolidification. The laser microtextured surface morphology consisted of tightly packed pillar-like surface features. The morphology of the microtexture was varied by controlling the laser processing parameters. The laser microtextured surface was coated with metallic particles using a thermal spray process. The tensile adhesive strength of the thermally sprayed metallic coating was higher by over 17% for a 5-μm deep microtexture, compared to that of grit-blasted samples. Also, this is the highest reported adhesion strength for laser-based microtexturing methods for thermally sprayed bond coatings.

Keywords Laser microtexturing · Thermally sprayed coating · Adhesion strength · Coatings · Laser processing

1 Introduction

Surface microtexturing has been utilized to improve the surface properties of materials. Some of the widely used surface microtexturing techniques are chemical etching, electrical discharge, and sandblasting [1]. Among the different surface microtexturing techniques, grit-blasting or sandblasting is a widely used method, but it does not allow selective roughening or generation of repeated patterns. Grit-blasting also leads to grit particle entrapment [2]. One of the alternative techniques for surface microtexturing is using a laser. Laser microtexturing can provide several advantages, easy automation, localized treatment, and three-dimensional profiles [3]. Surface microtexturing by laser is a low-cost and scalable method and eliminates the use of hazardous chemicals [4].

The adhesion strength between thermally sprayed metallic coating and the substrate improves when the surface is microtextured. Preparation of the substrates before being coated by the thermal spray process involves two steps: cleaning and roughening. Chemicals can be used to clean (degrease) the surface [5], while the roughening process can be performed by grit blasting or laser [6]. An increased coating contact area is favorable for increased adhesion bond strength. The laser wavelength, spot size, scanning rate, pulse duration, and pulse frequency can be optimized for enhanced adhesion [3]. However, low adhesion strength poses a serious problem to thermally sprayed coatings [7].

The formation of nanosecond laser-induced microtexture can be explained by localized surface melting, ablation, and the formation of superheated droplets around the solid surface [8]. The laser pulse energy density and frequency influence the shape and height of the surface features considerably. Increasing laser fluence and frequency results in the expulsion of more molten materials, which could lead

✉ Mool C. Gupta
mgupta@virginia.edu

Anustup Chakraborty
ac3xa@virginia.edu

Benjamin Chalfant
benjamin.chalfant@ccam-va.com

John Sions
john.sions@ccam-va.com

Ben Zimmerman
ben.zimmermann@ccam-va.com

[1] Charles L. Brown Department of Electrical and Computer Engineering, University of Virginia, Thornton Hall, 351 McCormick Road, Charlottesville, VA 22904, USA

[2] Commonwealth Center for Advanced Manufacturing, Disputanta, VA 23842, USA

to wider grooves and increased height of the resolidified surface microtexture. The laser parameters can be used to control the microtexture that influences the bonding strength of the thermal spray coatings.

Laser surface microtexturing improves the bond strength of thermally sprayed coatings by creating a mechanically interlocked bond between the substrate and the coating. Thermally sprayed metallic powder particles fill the pores on the surface created by laser microtexturing, and this results in a strong bond between the surface and the coating [9]. The thermally sprayed coating that is adhered to the surface by a mechanical interlocking mechanism has been classified into five types — embedding, anchoring, holding-on, spreading, and a mixture of several styles [10]. Depending on the material, both mechanical and physicochemical bonds can exist, and the bonding mechanism is influenced by particle–substrate contact time, contact temperature, and contact area upon impact [11]. It should also be noted that the adhesion strength is not only dependent on the contact area ratio and the density of the features but also varies with the microtexture shape and pattern [10, 12]. The thermal spray process parameters can also be optimized to enhance the adhesion strength as well. Adhesion strength can be significantly increased by increasing the particle velocity and keeping the particle temperature constant or by increasing the particle temperature and keeping the particle velocity at a fairly high constant value [13]. Other thermal spray process parameters, like gas flow rate and spray distance may also be optimized to get a potentially superior adhesion strength.

Among the most commonly used metals for the thermal spray process, aluminum has high-surface energy and provides strong resistance to corrosion in aggressive environments. Aluminum alloys have had a long history of usage in the construction, automotive, aviation, and astronautic industries [14, 15]. It greatly benefits from the favorable properties offered by adhesive bonding due to its excellent formidability and the high strength-to-weight ratio [14]. So, the focus of this study is on laser microtexturing of Al alloy Al-7075 and the improvement of adhesion strength of thermal spray coatings.

Extensive studies have been done on the adhesion strength of thermally sprayed coatings on surface microtextured aluminum alloys. A study on the improvement of adhesive bonding in aluminum alloys using surface microtexturing was done by Wong et al. [16] and Sharma et al. [17]. The substrates were grit-blasted using three different grit-blasting techniques, and the coating was deposited using the thermal spray process. Grit-blasted samples had significantly higher adhesion strength, compared to untextured samples. Kromer et al. [18] measured the tensile adhesion strength of NiAl powder coating on the Al 2017 substrates, as they are widely used in aircraft structural applications. NiAl powder with a mean particle size of 67 μm was thermally

sprayed onto the laser-textured aluminum alloy substrates. The adhesion test results showed that a decreasing density of holes on the metal surface causes a reduction in the adhesion strength of the thermally sprayed coating. The maximum reported adhesion strength was 52 MPa. Kromer et al. [7] also measured the adhesion strength of thermal spray coatings on grit-blasted and laser-microtextured aluminum alloy. A separate study was done by Kromer et al. [6], where laser microtextured and grit-blasted aluminum 2017 alloy samples were coated with NiAl powder (Amdry 956) using thermal spray. The samples were microtextured using a pulsed laser. Kromer et al. [6] also studied the strength of bond coats on a laser microtextured superalloy substrate. The maximum reported adhesive bond strength was 33 MPa. A recent study done by Zhang et al. [19] used a nanosecond pulsed laser to induce microtexture on the surface of aluminum alloy. This laser microtexture improved the bond strength of the Al-Cu aluminum alloy coating that was cold-sprayed on the aluminum alloy. The maximum reported bond strength was around 48 MPa. There is a need for further improvement of the adhesion strength of thermal spray coatings on Al alloys for long-duration operation.

In this paper, a full-area method of laser microtexturing is reported, and a superior coating adhesion strength of bond coats is demonstrated. The traditional laser microtexturing method is based primarily on the ablation process. The laser microtexturing process described in this paper is primarily based on the thermomechanical rearrangement of the molten material with very low ablation. The laser microtexturing is based on selecting the laser power in such a way that it offers melting combined with low ablation, and the laser beam is scanned over the entire surface area. Hence, a series of closely packed peaks and valleys are formed on the surface, which gives the thermally sprayed coating powder more grip due to enhanced surface area. The improvement in the coating adhesion strength would lead to increased longevity, robustness, and lower maintenance costs of metal parts and has potential applications in the automobile, power generation, and aerospace industries.

2 Experiment

2.1 Material

The substrates used were McMaster-Carr aluminum alloy (Al 7075) micromachined samples (diameter = 1 inch; thickness — 0.5 inches) polished down to a roughness of less than 1 μm. The chemical composition by weight of Al 7075 is supplied by the manufacturer and is given in Table 1. The coating powders used for the thermal spray process were Oerlikon Metco Amdry 995C (CoNiCrAlY) and Oerlikon Metco Amdry 9951 (Co[Ni]CrAlY). CoNiCrAlY is usually

Table 1 Al 7075 alloy composition (as obtained from the manufacturer)

Material Type	Al 7075
Al wt%	89.77
Zn wt%	5.4
Mg wt%	2.42
Cu wt%	1.42
Fe wt%	0.42
Cr wt%	0.21
Si wt%	0.13
Mn wt%	0.12

Table 2 Laser processing parameters (laser wavelength = 532 nm, scan speed = 60 mm/s, No. of scans = 1); line #1, line #2, and line #3 indicate the use of different process parameters

Pattern index	Frequency (kHz)	Fluence (J/cm^2)
Line #1	400	0.76
Line #2	400	0.92
Line #3	600	0.80

Table 3 Grit-blasting parameters

Blast media	Alumina (~ 50-μm particle size)
Pressure	0.28 MPa
Nozzle distance	~ 140 mm
Nozzle angle	70°
Nozzle traverse speed	1000 mm/s
Passes	2 orthogonal passes

used for bond coats [20–22]. The mean particle sizes of the powders were 90 μm and 38 μm, respectively. The different particle sizes were chosen to demonstrate the effect of particle size on surface morphology.

2.2 Laser microtexturing

A ytterbium fiber laser (YLP-G-10, IPG Photonics) of 532 nm wavelength, 10-W average power pulse width of 1.3 ns, pulse energy of 20.2 μJ, the repetition frequency of 600 kHz, and Gaussian beam profile was used in this study. The galvanometer scan head used was a SCANcube 14, SCANLAB, with a scan pattern designed in EZCad (Beijing JCZ Technology Co. Ltd). The laser repetition rate varied from 400 to 600 kHz, and a focused laser beam with a full width at a half-maximum (FWHM) size of 20 μm was used. The laser fluence used for the experiments was 0.76 J/cm^2, 0.92 J/cm^2, and 0.8 J/cm^2. The laser beam scan speed was maintained at 60 mm/s. For each laser fluence, the side-to-side overlap between the lines was 50%. The overlap between the laser spots along the direction of scanning was 99.25% and 99.5% at 400 kHz and 600 kHz, respectively. A galvanometer (SCANLAB SCANcube 14) controlled by a custom LabVIEW program was used to perform the raster scan of the aluminum surface. This enabled us to achieve

consistent microtexture patterns on the sample. A nitrogen gas atmosphere was used during laser microtexturing to prevent oxidation. The pressure of the gas was maintained at 5 MPa. A schematic diagram of the experimental setup is shown in Fig. 1. The different laser parameters used in the microtexturing process are shown in Table 2.

2.3 Grit blasting

The thermal spray coating samples were prepared on grit-blasted samples. For this process, the samples were secured to a plate using double-sided tape to ensure they remained stationary during abrasive blasting. The nozzle was rastered over the samples using the nominal parameters, as shown in Table 3. The raster scan was performed using a custom LabVIEW program on a computer using a controller that was connected to the nozzle. Thereafter, compressed air was

Fig. 1 Laser experimental setup with a galvanometer that can control laser scanning in 2D directions for laser processing of aluminum substrates
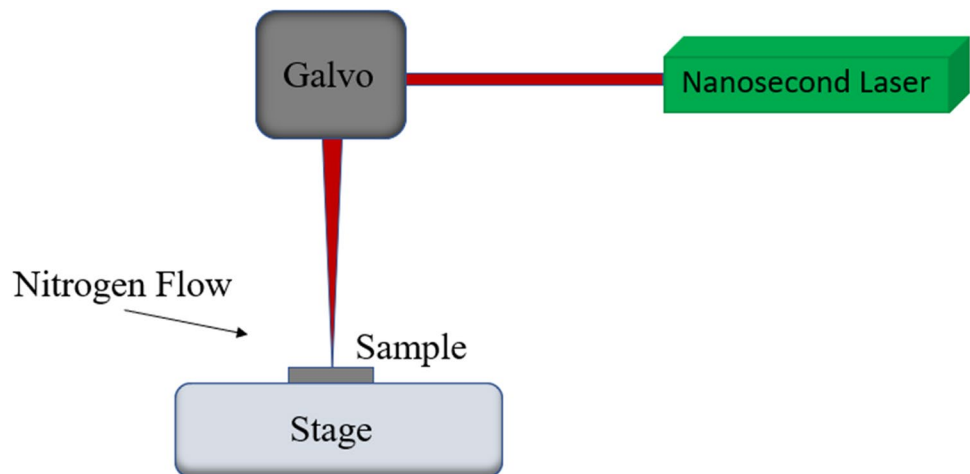
used on the samples to remove any residual dust. Then, the sample surface was cleaned with ethanol.

2.4 Thermal spray process

The grit-blasted and the laser microtextured samples were coated with metal powders by atmospheric plasma spray (APS) using an Oerlikon Metco F4MB-XL plasma gun attached to a 6-axis robotic arm. The first step of this process involved cleaning the grit-blasted and laser microtextured samples with compressed air. This was followed by attaching the samples to vertical fixtures. Thereafter, the thermal spray gun was turned on and passed over the substrate in a rectangular raster pattern. Before applying the powder, a pre-heat was executed to elevate the substrate temperature to 100 °C, and the powder feed was allowed to stabilize for 1–2 min before the deposition. Table 4 provides the different APS parameters used in this study.

2.5 Coating adhesion testing and failure analysis

The coated samples were subjected to tensile adhesion testing, where the tensile pressure required to debond the coatings was measured. This was done following the ASTM C633 standard using an Instron C633 mechanical analyzer. As shown in Fig. 2, the cylindrical sample was glued between two cylindrical rods. The load was applied in the direction perpendicular to the interface between the coating and the substrate. The tensile load was gradually increased until the coating was ruptured or detached from the substrate. The glue used in the process was Polyamide-epoxy FM 1000 Adhesive Film. The adhesion strength was
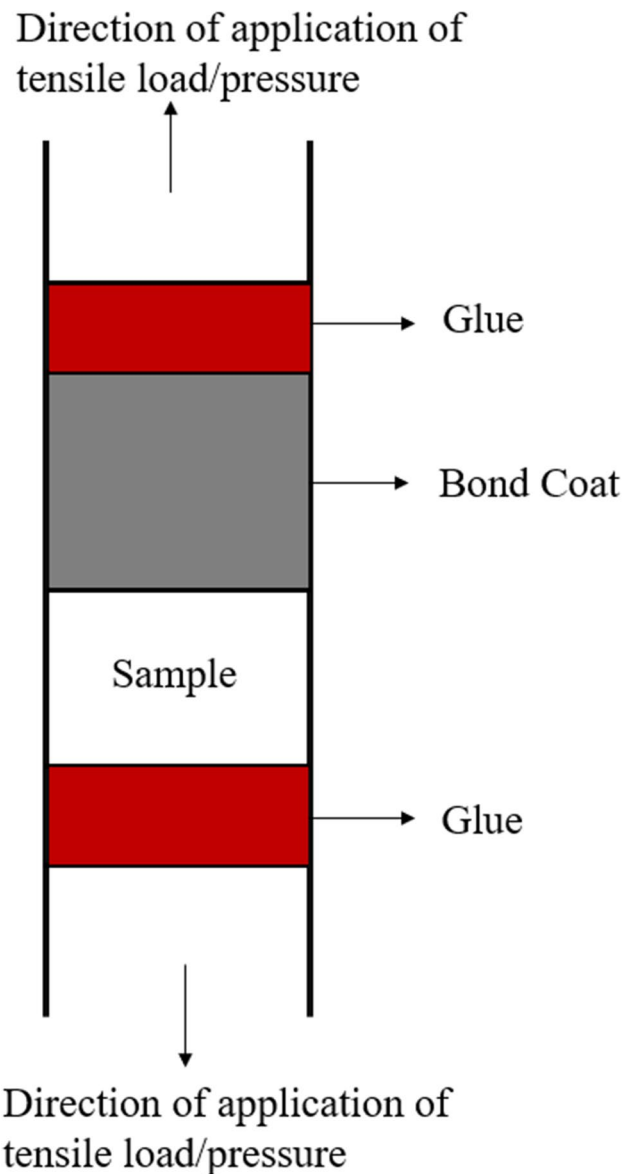

Fig. 2 Sample assembled for tensile adhesion testing; bond coat — coating layer that is attached to the sample; top coat — coating layer that is attached to the glue

calculated from the load at sample failure divided by the coating area [23].

2.6 Surface morphology and chemical composition characterization

The surface morphology and elemental analysis were done using FEI Quanta 650 Field Emission SEM. 3D optical profile measurements were done using an Olympus LEXT OLS4000 3D Laser Microscope to understand the variation in the microtexture heights, the peak-to-valley spacing, and the density and uniformity of the features. After the
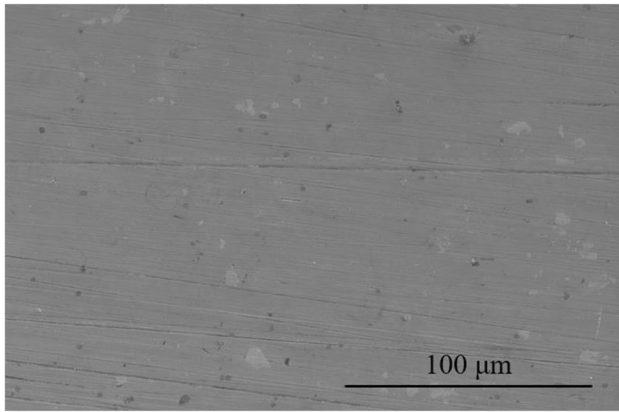
Table 4 Deposition parameters for a thermal spray for Amdry 9951 and 995C powders

APS parameters	Amdry 9951	Amdry 995C
Carrier gas	Argon	Argon
Carrier gas flow rate (nlpm)	4.5	3.5
Powder feeding rate (g/min)	60.5	60.1
Spray distance (mm)	120	120
Number of passes	10	10
Surface speed (mm/s)	1250	1250
Plasma temperature (°C)	2922	2612
Particle velocity (m/s)	210	166
Gun current (A)	600	600
Primary gas type	Argon	Argon
Primary gas flow rate (nlpm)	56.8	56.9
Secondary gas type	Hydrogen	Hydrogen
Secondary gas flow rate (nlpm)	8.5	57
Injector standoff distance (mm)	6	6
Water flow rate (lpm)	15.6	15.7

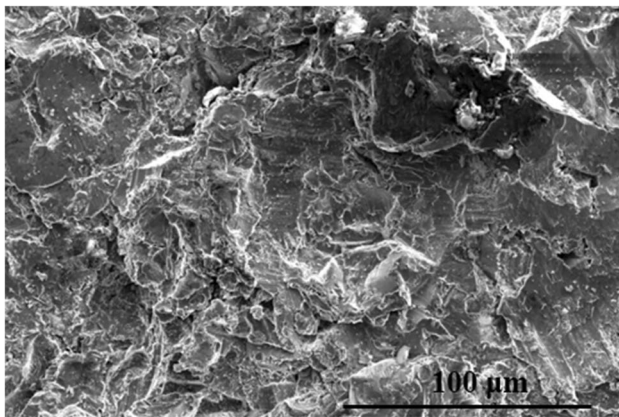**Fig. 3** SEM image of untextured Al 7075 surface

Fig. 4 SEM image of the surface of a grit-blasted sample

deposition of the coating, the cross-sectional morphology characterization and EDS analysis were also performed using the FEI Quanta 650 Field Emission SEM.

3 Results

3.1 Surface morphology

As a reference, Fig. 3 shows the surface of a plane untextured aluminum sample, while the surface of a grit-blasted sample is shown in Fig. 4. In grit-blasting, alumina particles hit the aluminum surface at a very high velocity, causing plastic deformation. The deformation is dependent on the velocity, shape, size, and hardness of the alumina particles [24].

Figure 5 shows the variation of the surface morphology with changing laser fluences. It can be seen that at higher laser fluences, the ablation is much more significant than at lower ones. The fluence at which the laser starts to mark features on the surface is between 0.38 J/cm^2 and 0.45 J/cm^2.

Figure 6 shows the variation of the surface morphology with changing laser repetition rate (frequency). Keeping the fluence constant, the number of laser pulses hitting the surface per second at a lower frequency is significantly less than that at a higher frequency. This provides less time for the molten surface material to cool down, resulting in higher temperatures and, subsequently, more ablation. Hence, the laser rearranges the molten material differently at higher frequencies compared to lower ones. As can be seen, the surface seems much more ablated and roughened at higher frequencies.

Figure 7 shows the different laser surface microtextured patterns. It can be seen that pillar-like structures have been formed on the surface with periodic grooves due to the thermomechanical process of melting and resolidification combined with some ablation. The thermally sprayed molten powders enter into the grooves and thus provide interlocking. The surface shown in Fig. 7(c) was obtained with the highest number of pulses per unit area, compared to the other two surfaces. The three laser microtextured patterns were chosen in such a way that it provides a range of variations in feature height and spacing between the peaks. Looking at the morphology, some resolidified droplet formation appears to occur, which further reinforces the process of melting, ablation, and resolidification of the material. On the other hand, the surface features reported by Kromer et al. [6, 7, 18] consist of a series of uniform holes drilled on the aluminum surface by laser ablation. Since the spacing between these holes was greater than 100 μm, the increase in the surface area was much less than that obtained by the full-area microtexturing method reported in this paper.

Figure 8 quantifies the micropillar height variations. The average height for the laser microtextured features was around 5 μm which is less than the average surface feature height of 6.5 μm for grit-blasted surfaces. There are considerable height variations on the laser microtextured and grit-blasted samples, with maximum heights reaching up to 27 μm, 28.2 μm, 41.6 μm, and 61.48 μm for line #1, line #2, line #3, and line #4 respectively. The average distance between the peaks in all the laser microtextured patterns was 5 μm. Compared to this, the depth of the laser-ablated holes on the aluminum surface reported by Kromer et al. [6, 7, 18] is 25–80 μm. Even though a larger hole depth results in a larger increase in surface area, it takes more time and does not always necessarily imply full infiltration by the thermally sprayed coating.

Figure 9 shows the surface morphology variation of a grit-blasted aluminum sample. It can be observed that there is no periodicity in the features formed on the surface as the grits impact the surface in a randomized manner.

Figures 10, 11, and 12 provide a detailed surface profile for the three laser microtexture patterns shown in Fig. 7. The 2D map shows the differences in height and density of the
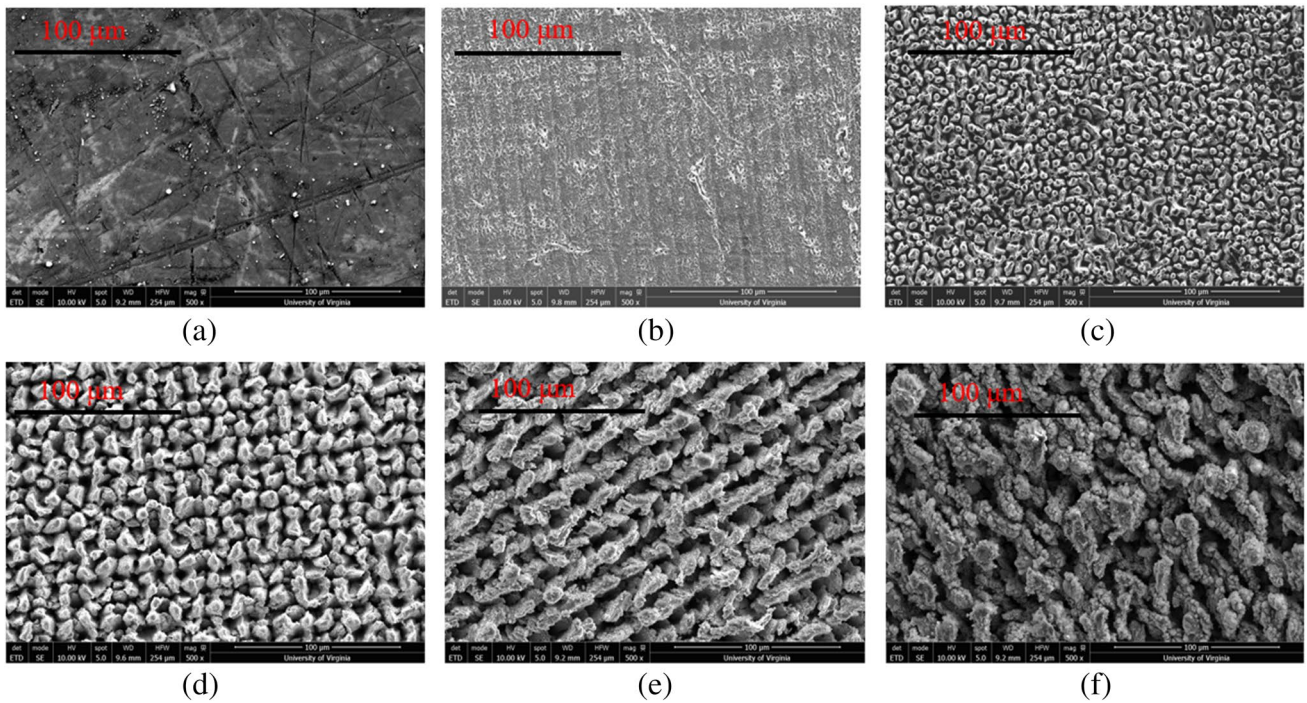
Fig. 5 a SEM image of untextured aluminum surface; SEM image of laser microtextured aluminum surface at a fluence of **b** 0.38 J/cm², **c** 0.45 J/cm², **d** 0.61 J/cm², **e** 0.76 J/cm², and **f** 0.91 J/cm². The frequency and the scanning speed were kept constant at 400 kHz and 60 mm/s, respectively

Fig. 6 SEM image of laser microtextured aluminum surface at **a** 20 kHz, **b** 200 kHz, **c** 300 kHz, and **d** 600 kHz. The laser fluence and the scanning speed were kept constant at 0.916 J/cm² and 60 mm/s, respectively

(a)   (b)   (c)
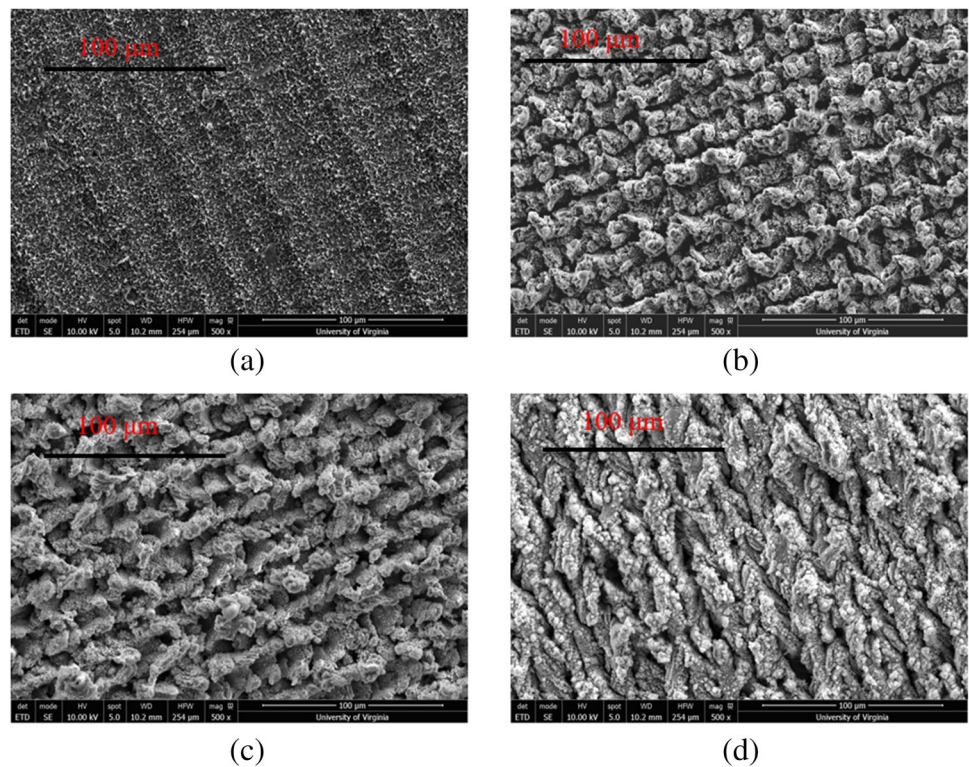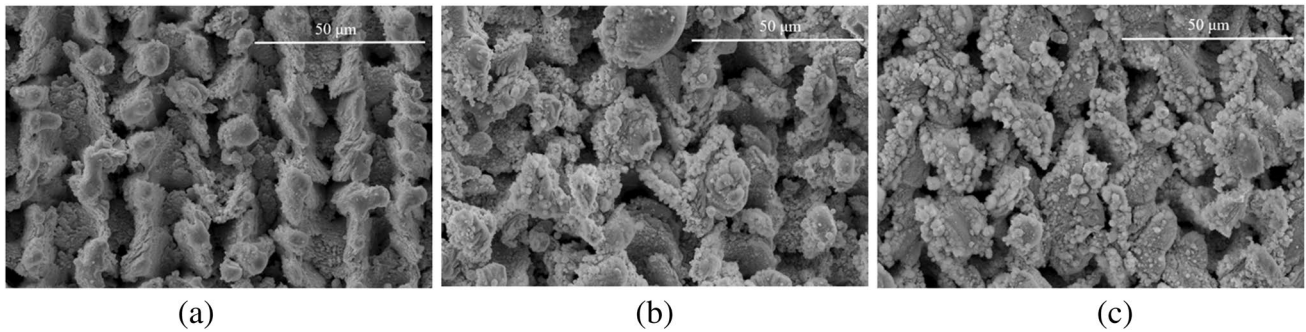
Fig. 7 **a** SEM image of laser microtextured (0.763 J/cm², 60 mm/s, and 400 kHz) aluminum sample; **b** SEM image of laser textured (0.916 J/cm², 60 mm/s, and 400 kHz) aluminum sample; **c** SEM image of laser microtextured (0.803 J/cm², 60 mm/s, and 600 kHz) aluminum sample
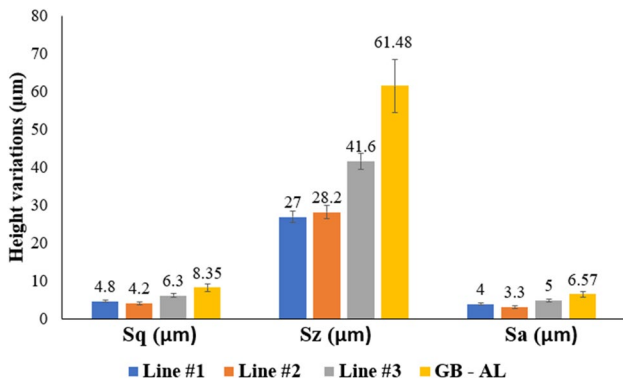

Fig. 8 Feature height variations on aluminum substrate. Line #1 — 0.763 J/cm², 60 mm/s, and 400 kHz; line #2 — 0.916 J/cm², 60 mm/s, and 400 kHz; and line #3 — 0.803 J/cm², 60 mm/s, and 600 kHz; GB — grit-blasted. Sq, RMS roughness; Sz, max peak to max valley distance; Sa, average roughness; The line # denotes the different laser parameters used

features across the surface, while the 3D map gives a more thorough visualization of the distribution of the features. It can also be observed that line #2 has higher peaks than those of line #1, and line #3 has higher peaks than those of line #1 and line #2. This can be attributed to the fact that line #3 had the highest number of laser pulses per unit area, and line #2 had more laser fluence than line #1. Since the scan speed was kept constant, the laser frequency and fluence are the two main factors controlling the height of the peaks on the surface. These two parameters are closely associated with each other in controlling the height of the micropillars.

The cross-sectional interface morphology of the laser microtextured samples (line #2) and the thermally sprayed coating are shown in Figs. 13 and 14. The EDS spectra in Figs. 13 and 14 show the oxygen concentration at the sample — Amdry 995C interface and sample-9951 interface. Even though nitrogen gas was constantly blown on the samples during the laser microtexturing process to displace the oxygen in the air, the samples still showed some oxidation. The oxidation could be further reduced by increasing the gas

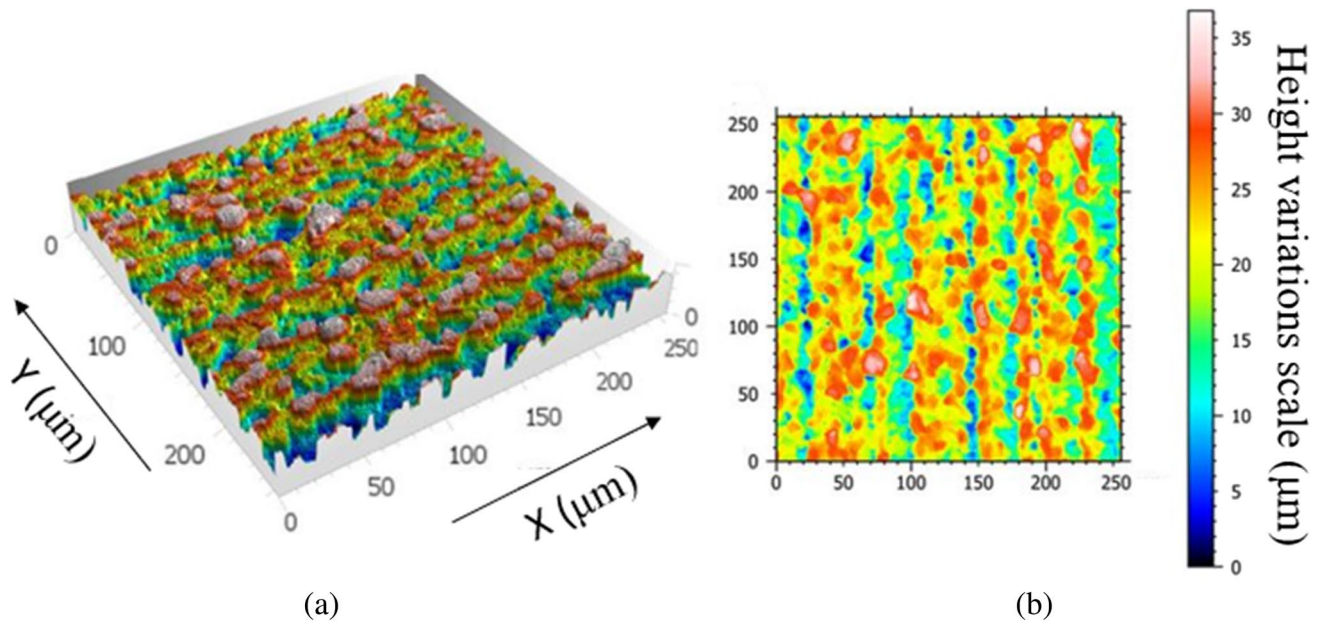**Fig. 9** 3D surface profile of a grit-blasted sample
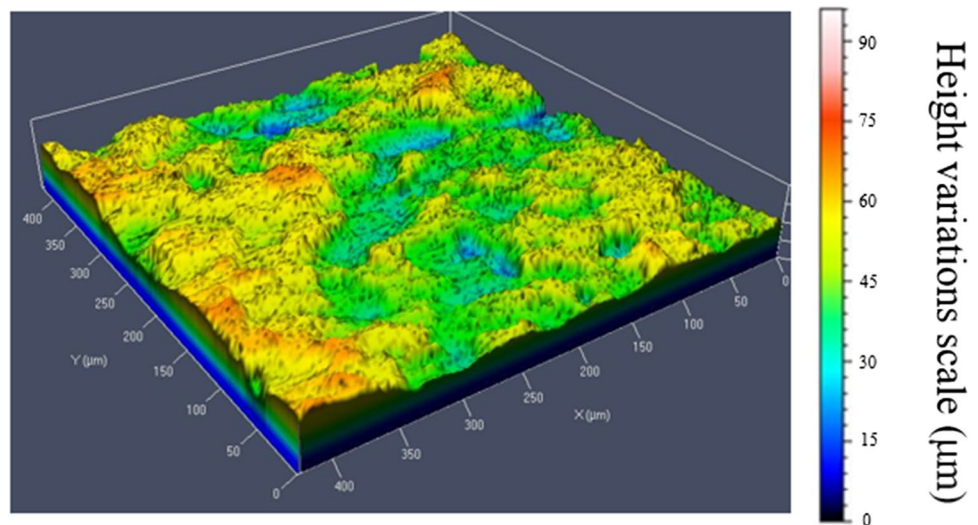
Fig. 10 **a** 3D surface profile of line #1 and **b** 2D surface profile of line #1; axis scales are in microns
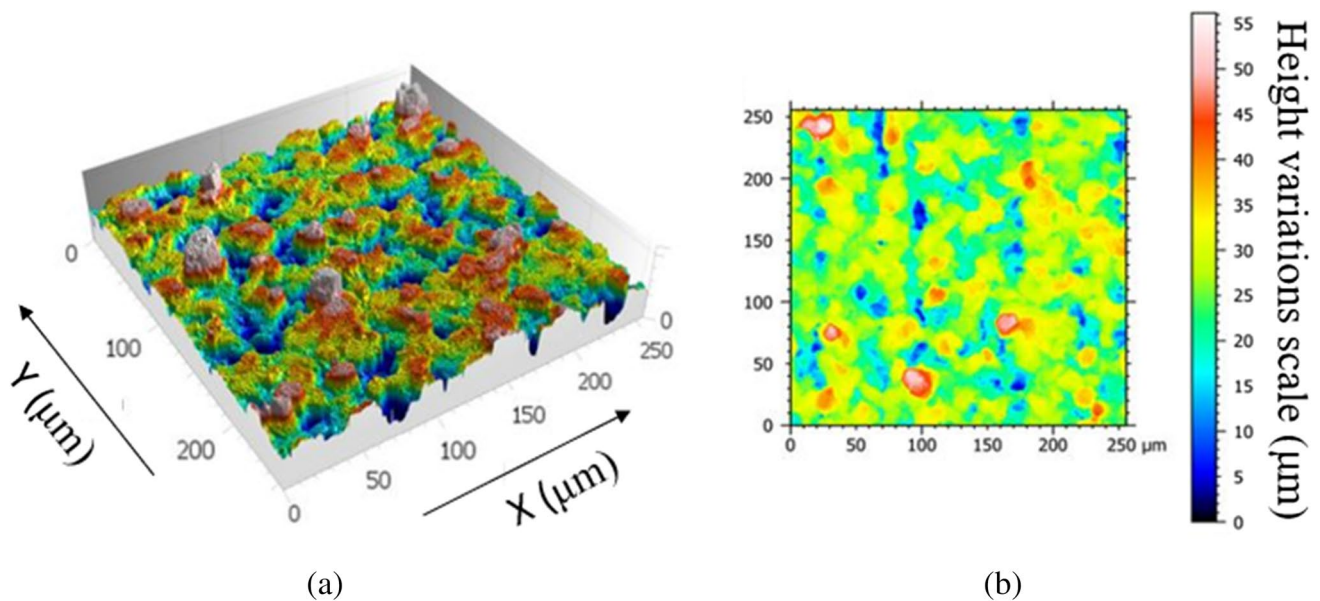

Fig. 11 **a** 3D surface profile of line #2 and **b** 2D surface profile of line #2; axis scales are in microns

flow rate on the surface of the sample. However, the samples would need to be in a vacuum to prevent oxidation entirely. Oxidation can also happen during the thermal spray process, depending on the thermal spray parameters and the kind of coating powder used.

Figure 15 shows the cross-sectional interface morphology of the grit-blasted sample and for thermal sprayed Amdry 995C particles. It can be seen that the coating on

the grit-blasted sample has much less infiltration than that on the laser microtextured surfaces. This is because of the absence of dense periodic grooves on the surface of the grit-blasted samples. Hence, even though the grit-blasted surface has the maximum peak-to-valley distance, its surface features are non-periodic and more spaced out, compared to those of the laser microtextured surfaces. The average thickness of the coating was found to be around 275 μm.
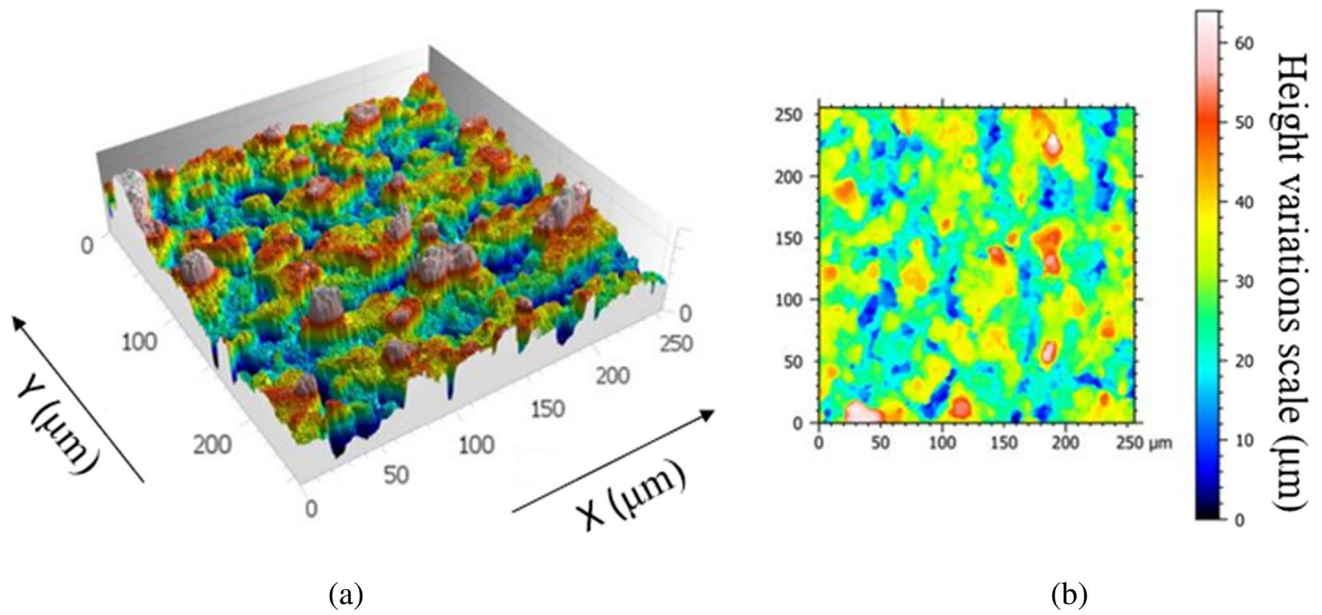
(a)

(b)

Fig. 12 **a** 3D surface profile of line #3 and **b** 2D surface profile of line #3; axis scales are in microns
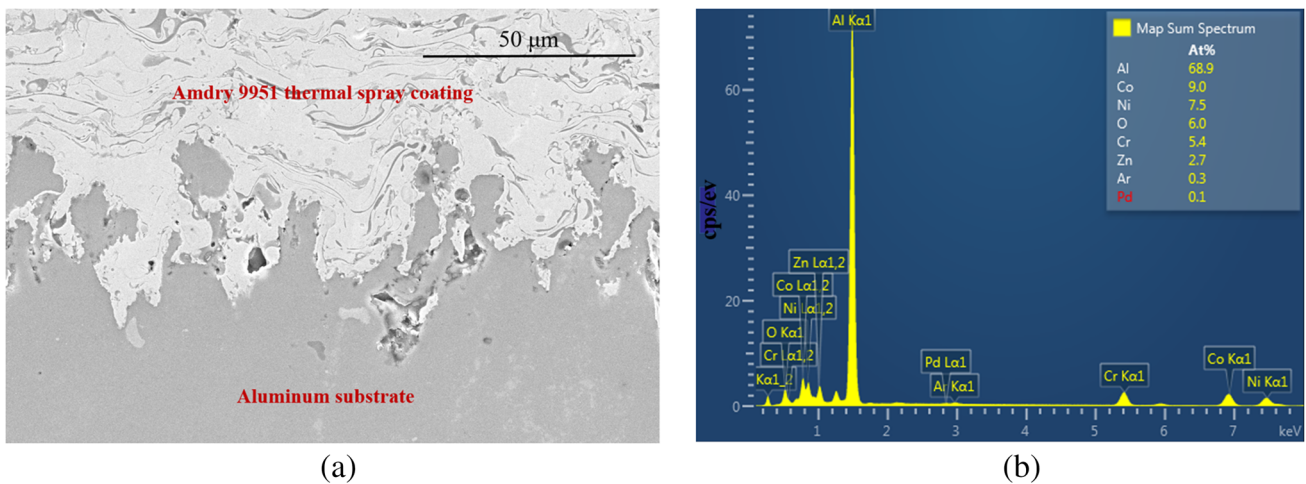

(a)

(b)

Fig. 13 **a** SEM cross-section image of the interface of line #3 and Amdry 9951; **b** EDS spectra showing the elemental composition of the interface of line #3 and Amdry 9951; and line #3 — 0.803 J/cm², 60 mm/s, and 600 kHz

3.2 Wettability and surface energy study

The water wettability and the surface energy of the laser microtextured surfaces were investigated using contact angle measurements. The measurements were done using a Ramè-hart Goniometer model 250. The surface energy of the aluminum was measured to be 852.46 ± 0.95 mN/m. The untextured aluminum surface was found to be mildly hydrophilic with water contact angles (CA) of $81° \pm 6°$. On the other hand, the laser microtextured aluminum surfaces were found to be highly hydrophilic,

exhibiting water contact angles of $25° \pm 8°$. This behavior can be explained by the fact that the water contact angle on a flat hydrophilic surface decreases with an increase in surface area, as expressed by Wenzel's equation [25, 26]:

$$\cos\Theta_r = r\cos\Theta_f \tag{1}$$

where Θ_f is the contact angle of water on an ideally smooth flat surface; Θ_r is the contact angle of water on a rough surface with r as the roughness parameter ($r = 1$ for smooth surfaces and $r > 1$ for rough surfaces).
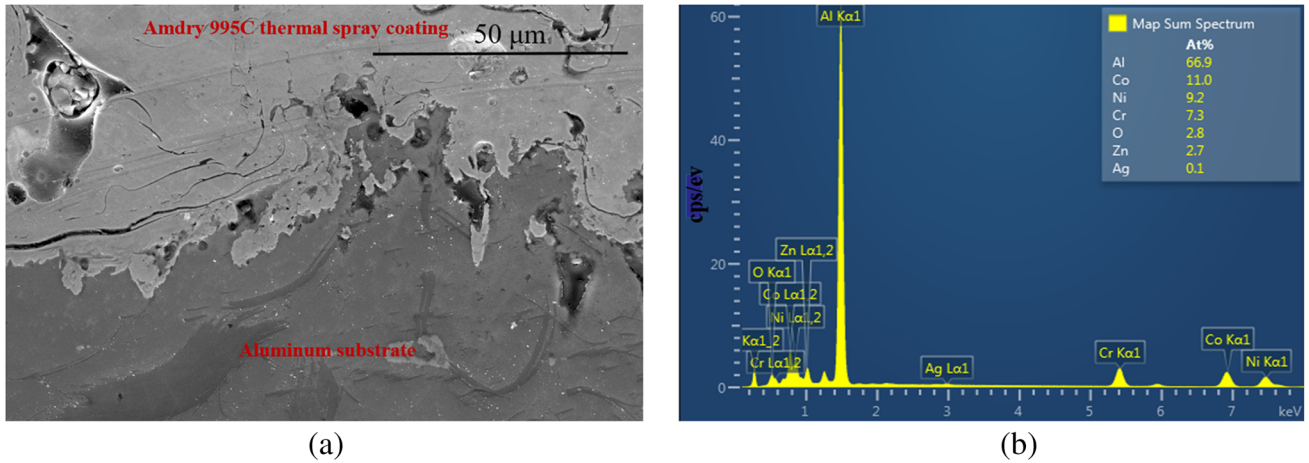
(a)

(b)

Fig. 14 **a** SEM cross-section image of the interface of line #3 and Amdry 995C; **b** EDS spectra showing the elemental composition of the interface of line #3 and Amdry 995C; and line #3 — 0.803 J/cm^2, 60 mm/s, and 600 kHz
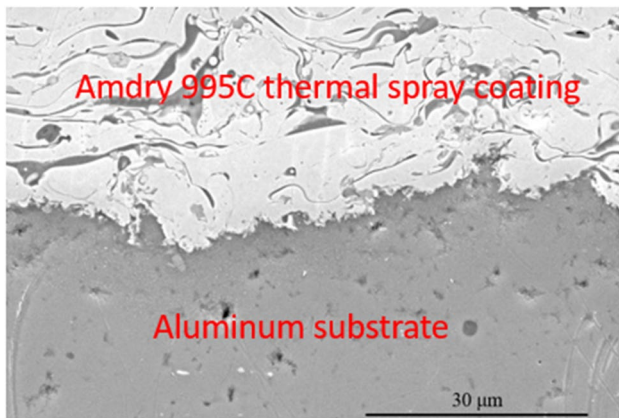

Fig. 15 SEM cross-section image of the interface of grit-blasted (GB) surface and Amdry 995C

3.3 Failure analysis

Figure 16 shows the thermally sprayed surface coating on the grit-blasted aluminum sample after the tensile adhesion test has been performed. Delamination can be observed across the surface of the coating in the case of the grit-blasted sample. The grit-blasted sample displayed cohesive failure at the epoxy-coating interface as well as adhesive failure, while the laser microtextured sample displayed only adhesive failure at the epoxy-thermal spray coating interface at the sample pull-off pressure.

3.4 Adhesion strength measurement results

We obtained significantly higher tensile adhesive strength for laser microtextured surfaces, compared to those reported in previous laser microtexturing research studies [6, 7, 17–19].
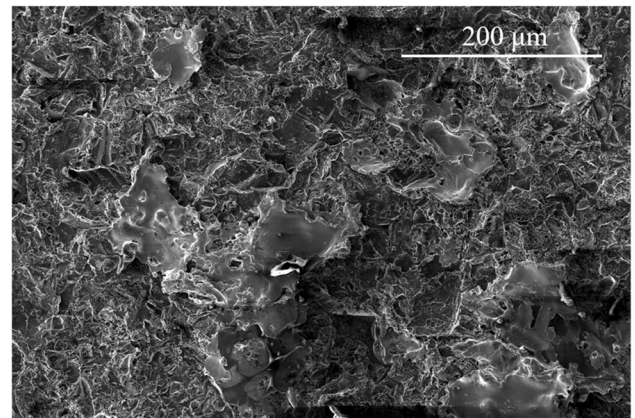

Fig. 16 Surface showing thermally sprayed coating on grit-blasted aluminum sample after tensile adhesion measurement test has been performed. Coating failure shows delamination of the thermally sprayed coating on a grit-blasted aluminum sample after the adhesion testing

Our results are shown in Fig. 17. Four samples were tested for each of the laser microtexturing and grit-blasting methods to obtain the adhesion data and the associated error bars. The laser microtextured patterns in our study were significantly denser than those reported in previous literature, as the laser was used to scan the surface area of the samples in its entirety. Thus, it can be proven that densely packed features are beneficial in increasing bonding strength.

4 Discussion

The features on the surface that are formed by melting, ablation, and resolidification of the materials are affected by the different laser parameters like fluence, pulse width, speed,

Fig. 17 Adhesion strength for grit-blasted and laser micro-textured samples. Line #1 — 0.763 J/cm², 60 mm/s, and 400 kHz; line #2 — 0.916 J/cm², 60 mm/s, and 400 kHz; line #3 — 0.803 J/cm², 60 mm/s, and 600 kHz; and line #4 — grit-blasted. Lines #1, #2, and #3 denote the different laser parameters used
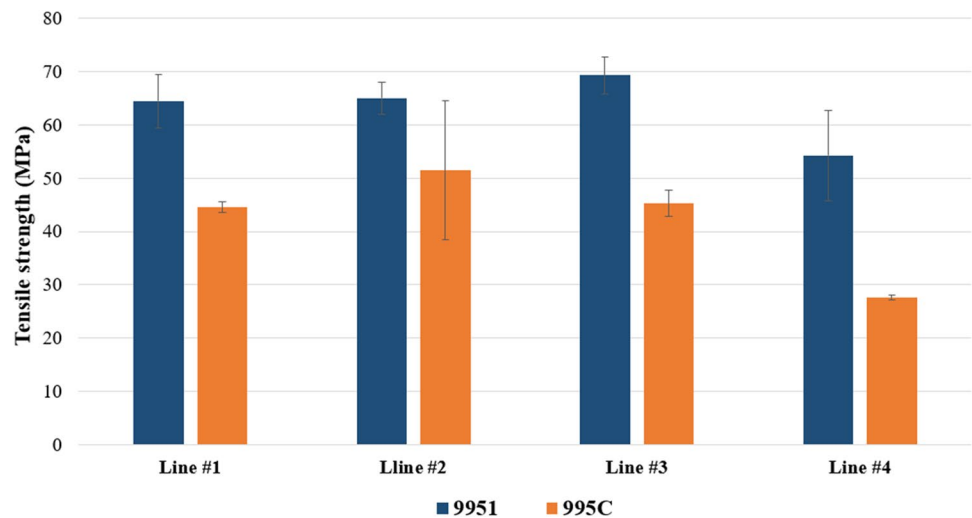
and frequency. The increase in laser frequency leads to an increased number of pulses per unit of surface area. This gives rise to deeper surface features, increased surface area, and hence, increased adhesion of the coating. The depth and density of the features can be controlled by changing the fluence and frequency of the laser. Moreover, higher laser power results in the ablation of more surface materials which leads to the formation of more particles. These particles can settle down and resolidify on top of the surface "pillars," providing nanoscale roughness which can further increase the adhesion of the coating. Feature height needs to be chosen so that the microtexture is stable under atmospheric plasma spray (APS) processing conditions.

The mechanism behind the formation of the pulsed laser-induced micropillars can be explained by ripple-like structures formed during the early stages of the microstructure evolution. Interference between the incident and the scattered laser light at the surface, heat-mass transfer, and hydrodynamic and plasmonic effects are the possible reasons behind the creation of the ripples. These ripples are broken down gradually as the microstructure develops, giving rise to the micropillars. The breaking down of the ripples can be attributed to molten material expansion and sputtering caused by the recoil pressure of the laser-matter interaction [27, 28]. The expelled molten material drops cool down drastically as soon as it leaves the laser-irradiated area. The effect of the recoil pressure on the molten material ceases to exist as the surface temperature drops below the vaporization point at the end of the laser pulse. Finally, gravitational forces and surface tension make the molten material settle back down on the surface [10].

The influence of the laser power density on the melt depth can be obtained by solving a one-dimensional heat conduction problem in the liquid and solid regions of the laser-irradiated area [29]. The penetration depth $X(t)$ can be expressed as a function of the laser power density I and irradiation time t as follows [29]:

$$X(t) = \left[-\frac{b_0}{2} + \left(\frac{b_0^2}{4} + \frac{a_0^3}{27} \right)^{1/2} \right]^{1/3} + \left[-\frac{b_0}{2} - \left(\frac{b_0^2}{4} + \frac{a_0^3}{27} \right)^{1/2} \right]^{1/3} - \frac{\alpha_l m_s}{16AI}$$

(2)

where

$$a_0 = \frac{3\alpha_l^2 m_s^2}{256(AI)^2} \left(\frac{192(AI)^2 t}{\alpha_l m_s^2} + 31 \right)$$

(3)

$$b_0 = -\frac{\alpha_l}{8AI} \left[\frac{\alpha_l^2 m_s^2}{256(AI)^2} \left(\frac{288(AI)^2 t}{\alpha_l m_s^2} + 47 \right) + \frac{t \left(18(AI)^2 t + 3\alpha_l m_s^2 \right)}{m_s} \right]$$

(4)

$$m_s = \rho \left[c_p (T_m - T_0) + L \right]$$

(5)

Here α_l is the thermal diffusivity in the liquid phase; T_m is the melting point; ρ is the density; c_p is the specific heat of materials in a solid phase; A is the absorptivity of materials; L is the latent heat of fusion; and T_0 is the initial temperature.

Furthermore, the temperature profile $T_s(x,t)$ in the solid metal region and the temperature distribution $T_l(x,t)$ in the liquid region is given as follows:

$$T_s(x,t) = T_m - (T_m - T_0) \left\{ 1 - \exp \left[-\frac{1}{\alpha_s} \frac{dX(t)}{dt}(x - X(t)) \right] \right\}, X(t) \le x < \infty$$

(6)

$$T_l(x,t) = T_m - \frac{AI}{k_l}[x - X(t)]$$
$$+ \frac{AI}{2\alpha_l k_l \left[1 + \frac{X(t)}{\alpha_l} \frac{dX(t)}{dt} \right]}$$
$$\times \frac{dX(t)}{dt}[x^2 - X^2(t)], 0 \le x \le X(t)$$

(7)

where x is the distance from the surface of the substrate; k_l is the thermal conductivity in the liquid phase; α_s is the thermal diffusivity in the solid phase; and AI is the absorbed laser power density.

The influence of the laser power density on the melt depth can be obtained by solving a one-dimensional heat conduction problem in the liquid and solid regions of the laser-irradiated area [29].

It should be noted that for all the laser microtextured and even the grit-blasted surfaces, the adhesion strength of Amdry 9951 powder is more than that of Amdry 995C powder. This is because the mean particle size of Amdry 9951 powder is much smaller, compared to Amdry 995C powder. This allows for increased infiltration of the molten particles into the laser-generated microtexture, thereby providing more tensile adhesive strength, as shown in Fig. 18. Optimizing coating-substrate adhesion requires adaptation of the powder size to the surface topography to achieve a superior surface filling ratio [9]. The average laser-formed feature height in this work was around 5 μm, compared to feature depths of 80–180 μm reported in previous laser studies [6, 7]. Hence, the throughput of the full-area laser microtexturing method is higher, and the associated cost will be much lower.

Compared to grit-blasting, which only provides macroscale roughness, the fully microtextured laser method provides superior control and micro-scale roughness. The maximum adhesion strength reported in the scientific literature for thermally sprayed Amdry 9951 (CoNiCrAlY) bond coat to laser microtextured surface is around 52 MPa [18]. This value is comparable to that of the measured grit-blasted samples, which is around 55 MPa. In this paper, we have demonstrated the adhesion strength of bond coat to laser

microtextured samples of 65 MPa, which is an increase of around 17%.

Some of the other potential applications of improved adhesion strength thermal spray coatings include oxidation and hot corrosion resistance of airfoils, turbine buckets, ceramic clearance control coatings, exhaust manifolds, flue gas, and fly ash systems. So, the method of surface microtexturing presented in this paper could have a wide range of varied applications in improving the adhesion strength of thermally sprayed coatings on other metals and alloys.

5 Conclusion

The key points presented in this paper are as follows:

(i) This paper demonstrates a novel method for laser microtexturing through a thermomechanical process of creating dense, uniform pillar-like features for the improvement of coating adhesion strength. The entirety of the area of the surface was laser microtextured by forming densely populated micropillars, and this led to an increase of around 65% in the total surface area. The micro "pillar"-like shape of the microtexture significantly increases the contact area ratio, and this led to a substantial increase in the adhesion strength of atmospheric plasma sprayed metallic coatings.

(ii) The control of laser power and frequency allowed the variation of micropillar height to over 40 μm. The micropillars contributed to a substantial increase in the atmospheric plasma sprayed coating adhesion strength, compared to untextured, grit-blasted, and
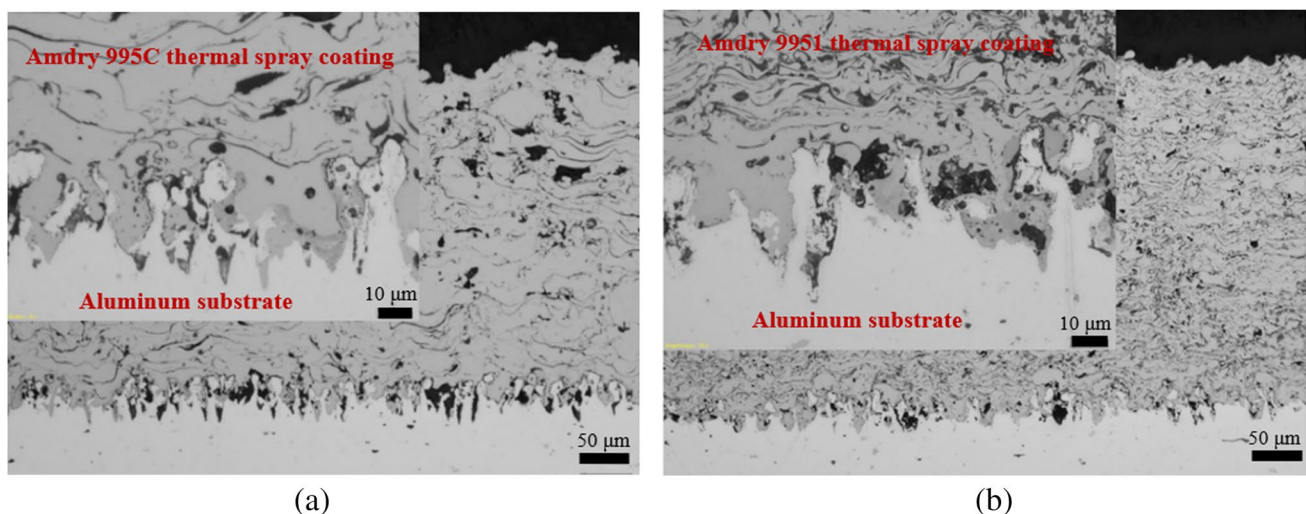

Fig. 18 Interface showing **a** infiltration of Amdry 995C powder on laser microtextured surface and **b** infiltration of Amdry 9951 on laser microtextured surface. Infiltration of Amdry 9951 into the grooves is much more than that of 995C due to the smaller mean particle size

other laser microtextured surfaces, as reported in the literature.

(iii) The increase in bond strength was measured and explained due to thermally sprayed particles filling the gap between the pillars. The results of the laser microtexturing process parameter's effect on surface morphology are reported. The cross-section of the thermally sprayed coating of laser microtextured surfaces was studied to provide an understanding of adhesion strength improvements.

Declarations

Competing interests The authors declare no competing interests.

References

1. Lamraoui A, Costil S, Langlade C, Coddet C (2010) Laser surface texturing (LST) treatment before thermal spraying: a new process to improve the substrate-coating adherence. Surf Coat Technol 205:164–167. https://doi.org/10.1016/j.surfcoat.2010.07.044

2. Bagade VU, Duraiselvam M, Sarangi N (2022) Effect of laser surface texturing on coating adherence and tribological properties of CuNiIn and MoS_2 coating. Trans Indian Inst Met 75:239–250. https://doi.org/10.1007/s12666-021-02417-0

3. Kromer R, Danlos Y, Aubignat E, Verdy C, Costil S (2017) Coating deposition and adhesion enhancements by laser surface texturing – metallic particles on different classes of substrates in cold spraying process. Mater Manuf Process 32:1642–1652. https://doi.org/10.1080/10426914.2017.1364750

4. Mulroney AT, Gupta MC (2017) Optically transparent superhydrophobic polydimethylsiloxane by periodic surface microtexture. Surf Coat Technol 325:308–317. https://doi.org/10.1016/j.surfcoat.2017.06.066

5. Garcia-Alonso D, Serres N, Demian C, Costil S, Langlade C, Coddet C (2011) Pre-/during-/post-laser processes to enhance the adhesion and mechanical properties of thermal-sprayed coatings with a reduced environmental impact. J Therm Spray Technol 20:719–735. https://doi.org/10.1007/s11666-011-9629-x

6. Kromer R, Costil S, Cormier J, Courapied D, Berthe L, Peyre P, Boustie M (2015) Laser surface patterning to enhance adhesion of plasma sprayed coatings. Surf Coat Technol 278:171–182. https://doi.org/10.1016/j.surfcoat.2015.07.022

7. Kromer R, Costil S, Verdy C, Gojon S, Liao H (2018) Laser surface texturing to enhance adhesion bond strength of spray coatings – cold spraying, wire-arc spraying, and atmospheric plasma spraying. Surf Coat Technol 352:642–653. https://doi.org/10.1016/j.surfcoat.2017.05.007

8. Long J, Cuo Z, Lin C, Zhou C, He Z, Xie X (2019) Formation mechanism of hierarchical micro- and nanostructures on copper induced by low-cost nanosecond lasers. Appl Surf Sci 464:412–421. https://doi.org/10.1016/j.apsusc.2018.09.055

9. Kromer R, Cormier J, Costil S (2016) Role of powder granulometry and substrate topography in adhesion strength of thermal spray coatings. J Therm Spray Technol 25:933–945. https://doi.org/10.1007/s11666-016-0411-y

10. Tan N, Xing Z, Wang X, Wang H, Jin G, Xu B (2017) Effects of texturing patterns on the adhesion strength of atmosphere plasma sprayed coatings. J Mater Res 32:1682–1692. https://doi.org/10.1557/jmr.2017.164

11. Kromer R, Danlos Y, Costil S (2018) Cold gas-sprayed deposition of metallic coatings onto ceramic substrates using laser surface texturing pre-treatment. J Therm Spray Technol 27:809–817. https://doi.org/10.1007/s11666-018-0718-y

12. Zhan X, Liu Y, Yi P (2021) Effect of substrate surface texture shapes on the adhesion of plasma-sprayed Ni-based coatings. J Therm Spray Technol 30:270–284. https://doi.org/10.1007/s11666-020-01126-2

13. Lyphout C, Nylén P, Östergren LG (2011) Relationships between process parameters, microstructure, and adhesion strength of HVOF sprayed IN718 coatings. J Therm Technol 20:76–82. https://doi.org/10.1007/s11666-010-9543-7

14. Spadaro C, Sunseri C, Dispenza C (2007) Laser surface treatments for adhesion improvement of aluminum alloys structural joints. Radiat Phys Chem 76:1441–1446. https://doi.org/10.1016/j.radphyschem.2007.02.047

15. Kadleckova M, Minarik A, Smolka P, Mracek A, Wrzecionko E, Novak L, Musilova L, Gajdosik R (2018) Preparation of textured surface on aluminium-alloy substrates. Materials (Basel) 12:109–120. https://doi.org/10.3390/ma12010109

16. Wong RCP, Houk AP, Kim JK, Yu TX (1997) Improvement of adhesive bonding in aluminum alloys using a laser surface texturing process. J Mater Process Technol 63:579–584. https://doi.org/10.1016/S0924-0136(96)02687-8

17. Sharma MM, Eden TJ, Golesich BT (2015) Effect of surface preparation on the microstructure, adhesion, and tensile properties of cold-sprayed aluminum coatings on AA2024 substrates. J Therm Spray Technol 24:410–422. https://doi.org/10.1007/s11666-014-0175-1

18. Kromer R, Costil S, Cormier J, Berthe L, Peyre P, Courapied D (2016) Laser patterning pretreatment before thermal spraying: a technique to adapt and control the surface topography to thermomechanical loading and materials. J Therm Spray Technol 25:401–410. https://doi.org/10.1007/s11666-015-0352-x

19. Zhang C, Zhang D, Luo C, Peng W, Zang X (2021) Nanosecond pulse laser assisted cold spraying of Al–Cu aluminum alloy. Coatings 11:267–272. https://doi.org/10.3390/coatings11030267

20. Lima CRC, Guilemany JM (2007) Adhesion improvements of thermal barrier coatings with HVOF thermally sprayed bond coats. Surf Coat Technol 201:4694–5470. https://doi.org/10.1016/j.surfcoat.2006.10.005

21. Crespo V, Cano IG, Dosta S, Guilemany JM (2015) The influence of feedstock powders on the CGS deposition efficiency of bond coats for TBCs. J Alloys Compd 622:394–401. https://doi.org/10.1016/j.jallcom.2014.09.216

22. Karaoglanli AC, Dikici H, Kucuk Y (2013) Effects of heat treatment on adhesion strength of thermal barrier coating systems. Eng Fail Anal 32:16–22. https://doi.org/10.1016/j.engfailanal.2013.02.029

23. ASM Thermal Spray Society (TSS), Accepted practice to test bond strength of thermal spray coatings. https://www.asminternational.org/documents/17679604/17683439/AcceptedPracticeBondStrengthApprovedformatted_Intro.pdf/4bcf5903-414d-413f-ab69-7cf0cc9123bd. Accessed 24 Aug 2021

24. Lambiase F, Liu F (2022) Recent advances in metal-polymer joining processes. In Rakesh P, Davim P (ed) Mechanical engineering series, joining processes for dissimilar and advanced materials, 3rd edn. Woodhead Publishing Reviews: Mechanical Engineering Series, pp 123–151

25 Wenzel RN (1936) Resistance of solid surfaces to wetting by water. Ind Eng Chem 28:988–994. https://doi.org/10.1021/ie50320a024

26. Madry K, Nowicki W (2021) Wetting between Cassie-Baxter and Wenzel regimes: a cellular model approach. Eur Phys J E 44: 138–149. https://link.springer.com/article/10.1140/epje/s10189-021-00140-8

27. Nayak BK, Gupta MC (2010) Self-organized micro/nano structures in metal surfaces by ultrafast laser irradiation. Opt Lasers Eng 48:940–949. https://doi.org/10.1016/j.optlaseng.2010.04.010

28. Zhang J, Zhang S, Chen G, Jia Z, Qu Y, Guo Z (2022) Laser micro-texture formation mechanism based on modified heat-mass transfers and hydrodynamic models. Int J Mech Sci 230:107528–107538. https://doi.org/10.1016/j.ijmecsci.2022.107528

29. Xie J, Kar A (1997) Mathematical modeling of melting during laser materials processing. J Appl Phys 81:3015–3022. https://doi.org/10.1063/1.364336